Arab J Sci Eng (2014) 39:8559–8572
DOI 10.1007/s13369-014-1436-5

RESEARCH ARTICLE - CIVIL ENGINEERING

New Insight into Interaction of Buckling Modes with Stable Post-buckling Response

Charis J. Gantes · Maria A. Livanou · Tassos P. Avraam

Received: 19 June 2014 / Accepted: 31 August 2014 / Published online: 12 November 2014

Abstract Buckling mode interaction of elastic systems in the presence of initial imperfections is well known to have a detrimental effect on the response of a wide range of structural systems. This has been demonstrated mostly analytically for simple models, assuming small displacements, thus obtaining results with questionable validity in the post-buckling range. In order to acquire additional insight into this issue, in the first part of the present paper, two different versions of the well-known 2-DOF Augusti model, whose independent buckling modes are both stable, are studied analytically without any simplifying assumptions with respect to the magnitude of deformation, in order to accurately demonstrate the coupling phenomena in the presence of imperfections in the pre- and post-buckling range. Depending on the nature of the structure's rotational springs, its post-buckling equilibrium path may be either stable or unstable. Afterward, the elastic response of two examples of laced built-up columns is illustrated numerically, one characterized by interaction between in-plane global and local buckling and the other by in- and out-of-plane global buckling, featuring similar response to that of the two 2-DOF models, respectively, thus demonstrating occurrence of such behavior in actual structural systems.

C. J. Gantes · M. A. Livanou (✉) · T. P. Avraam
Metal Structures Laboratory, Department of Civil Engineering, National Technical University of Athens, Zografou Campus, 9, Iroon Polytechneiou Street, 15780 Athens, Greece
e-mail: livanoumaria@gmail.com

C. J. Gantes
e-mail: chgantes@central.ntua.gr

T. P. Avraam
e-mail: avraamt@central.ntua.gr

Keywords Buckling mode interaction · Two-DOF system · Imperfections · Post-buckling behavior · Stability · Laced built-up column

الخلاصة

من المعروف بشكل جيد أن تداخل نمط الالتواء للأنظمة المرنة في وجود عيوب أولية له تأثير ضار في استجابة مجموعة واسعة من الأنظمة الهيكلية. وقد تم توضيح هذا الأمر في الغالب تحليليا لنماذج بسيطة ، على افتراض وجود إزاحات صغيرة ، وبالتالي الحصول على نتائج مع صحة مشكوك فيها لنطاق ما بعد الالتواء. ومن أجل الحصول على نظرة إضافية على هذه المسألة تم تحليليا -في الجزء الأول من هذه الورقة العلمية -دراسة إصدارين مختلفين من نموذج أوجستي ذي درجتين من الحرية المعروف جيدا وتكون فيه جميع أنماط الالتواء المستقلة مستقرة دون أي افتراضات تبسيط فيما يتعلق بحجم التشوه، وذلك من أجل إظهار ظواهر الاقتران بدقة بوجود عيوب في نطاق ما قبل وبعد الالتواء. وتبعا لطبيعة نوابض الهيكل الدورانية، فإنه ربما يكون مسار الاتزان بعد الالتواء الخاص به مستقرا أو غير مستقر. وتم بعد ذلك عدديا توضيح الاستجابة المرنة لمثالين من الأعمدة المبنية ذات الأربطة، واحدة تتميز بالتداخل بين الالتواء في المستوى العالمي والمحلي والآخر هو التواء عالمي في وخارج المستوى ، ويضم استجابة مماثلة لتلك التي من كلا النموذجين ذي اثنتين من درجات الحرية ، على التوالي ، مما يدل على حدوث مثل هذا السلوك في النظم الهيكلية الفعلية.

1 Introduction

Optimizing the weight of a structure based on the first critical buckling load of the perfect structure may often produce a design for which the critical loads for several buckling modes coincide [1]. It is well known that if the critical loads corresponding to at least two buckling modes are equal, or nearly so, the elastic post-buckling response involves coupling between them [2]. The phenomenon of buckling mode interaction has been first studied by Koiter [3] and later by Chilver [2] and Supple [4] for 2-DOF systems and by Johns and Chilver [5] for N-DOF systems, without taking into account the presence of initial imperfections.

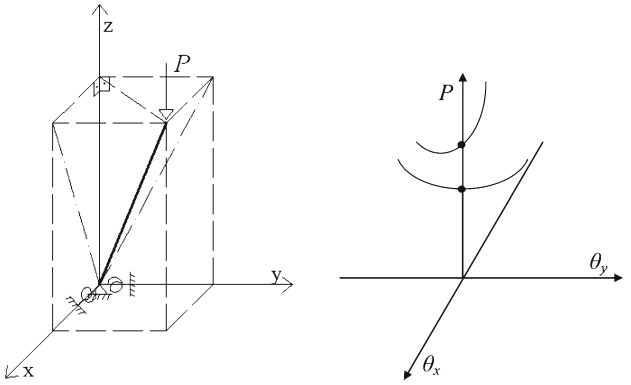

Fig. 1 **a** Geometry of examined model and **b** stable post-buckling equilibrium paths of the two independent buckling modes

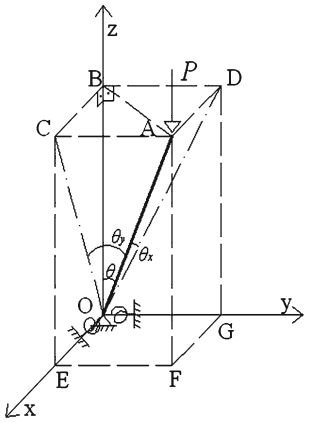

Fig. 2 Geometry of the first 2-DOF model

At the same time, many researchers investigated the effect of initial imperfections on the buckling of elastic structures. Koiter [3] has shown that the critical load of a structure which loses its stability at a bifurcation point may be extremely sensitive to the presence of small imperfections, leading to the conversion of a bifurcation point into a limit point occurring at a lower load. Roorda [6] showed that the effect of small initial imperfections on the limit point load is largely dependent on the slope of the initial post-buckling curve of the perfect system and that the change in limit point load varies with the square root of initial imperfections. Similarly, many other authors, such as Ho [7] and Thompson [8] studied the same issue.

The phenomenon of buckling mode interaction leads to increased imperfection sensitivity [1]. The effect of coexistence of coupled buckling and imperfections in elastic structures has been investigated by Supple [9], Ho [10,11] and Johns [12]. A thorough review of the general theory of coupled instabilities in the presence of imperfections has been previously presented by Gioncu [13].

The present paper deals with the buckling mode interaction of elastic systems and the effect of initial imperfections on their behavior. More specifically, two different versions of a 2-DOF model initially introduced by Augusti [14] are studied analytically via the energy method, accounting for geometrical nonlinearities and without making any mathematical simplifications during the solution process, thus accounting for arbitrarily large displacements. The model consists of a cantilever rigid rod, with fully restrained displacements and elastically restrained rotations at the bottom, subjected to a concentrated load at the top, which retains its direction throughout the analysis (Fig. 1a). The two independent buckling modes of this system present both stable post-buckling equilibrium paths (Fig. 1b).

In the second part of the paper, two examples of built-up columns, which are well known to exhibit buckling mode interaction [1], are presented and their structural behavior is demonstrated by means of geometrically nonlinear finite element analyses carried out with software ADINA [15]. In the first example, the in-plane elastic behavior of a simply supported laced built-up column is studied, for which the two first modes, representing local buckling of the column flanges and in-plane global buckling, exhibit stable post-buckling equilibrium paths. In the second example, a similar built-up column is studied but the geometry and section of the flanges are appropriately chosen in order to avoid in-plane local buckling. Thus, interaction between in- and out-of-plane global buckling is investigated in the presence of imperfections. Both of them individually present stable post-buckling response. Initial results of this research have been recently presented by the authors [16].

2 2-DOF Model with Unstable Post-buckling Behavior

In the first 2-DOF model, the two rotational springs are considered to have reactions proportional to the angles AOD $=$ θ_x and AOC $=$ θ_y of the rod with its projections on the planes yz and xz, respectively (Fig. 2). In the case of initial imperfections, denoted by corresponding inclination ε_x and ε_y of the rod with respect to the vertical position, the springs are considered to be undeformed; thus, their reactions are zero in the initial inclined position of the rod. The deformation is expressed with respect to the two rotational degrees of freedom θ_x and θ_y, and the equilibrium equations are derived by means of the energy method, taking into consideration geometrical nonlinearities. In the following sections, the formulation of the model's equilibrium equations and their numerical treatment are presented.

2.1 Formulation of Equilibrium Equations

The geometry of the model is illustrated in Fig. 2. The rod's length is equal to L. The springs exhibit linearly elastic re-

sponse, with rotational stiffness coefficients c_x and c_y in x and y direction, respectively. The critical loads corresponding to the two independent buckling modes of the system, which exhibit stable post-buckling response [14], are $P_{\mathrm{cr},x} = c_x/L$ and $P_{\mathrm{cr},y} = c_y/L$. In an arbitrary position, the rod forms with the vertical axis z angle equal to θ, while the corresponding initial angle is equal to ε.

By geometrical formulations, and without making any simplifying assumption, the exact relationship describing the geometry of the system is derived:

$$\cos\theta = \sqrt{1 - \sin^2\theta_y - \sin^2\theta_x} \tag{1}$$

The total potential energy Π of the system can then be written as:

$$\Pi = \frac{1}{2}c_x(\theta_x - \varepsilon_x)^2 + \frac{1}{2}c_y(\theta_y - \varepsilon_y)^2 - PL(\cos\varepsilon - \cos\theta) \tag{2}$$

By setting equal to zero, the derivatives of the total potential energy with respect to the two degrees of freedom θ_x and θ_y, and by normalizing the external force P with respect to the critical buckling load $P_{\mathrm{cr},y} = c_y/L$, the following equilibrium equations are obtained:

$$\frac{\partial\Pi}{\partial\theta_x} = \frac{c_x}{c_y}(\theta_x - \varepsilon_x) - \lambda\frac{\sin\theta_x\cos\theta_x}{\sqrt{1 - \sin^2\theta_x - \sin^2\theta_y}} = 0 \tag{3}$$

$$\frac{\partial\Pi}{\partial\theta_y} = (\theta_y - \varepsilon_y) - \lambda\frac{\sin\theta_y\cos\theta_y}{\sqrt{1 - \sin^2\theta_x - \sin^2\theta_y}} = 0 \tag{4}$$

where $\lambda = P/P_{\mathrm{cr},y}$ is the normalized load. Each triad θ_x, θ_y, λ that satisfies the above equations, constitutes an equilibrium position of the system.

2.2 Numerical Treatment of Equilibrium Equations

The numerical solution of Eqs. (3), (4) was carried out by means of MATLAB software [17]. A simplified version of the basic principle of the arc length method [18] has been applied, searching for a solution on the surface of a properly selected sphere, in order to capture possible snap-through or snap-back phenomena. Therefore, three simultaneous nonlinear equations, the two equations of equilibrium and the geometrical equation of the sphere, are solved with respect to the variables θ_x, θ_y, λ. At every step, the previous triad of solutions is selected as the new sphere's center, while its radius is assigned a small positive value. Convergence tests of the nonlinear solution algorithm have been performed, to ensure that the solution step is sufficiently small and that there is numerical stability. The non-linear system of equations has been solved successively for different values of the control parameters, which are chosen to be:

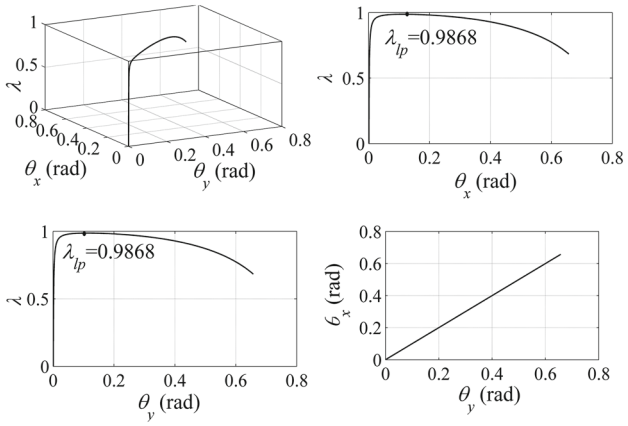

Fig. 3 Equilibrium paths of first 2-DOF model for $R_{\mathrm{P}} = 1.00$, $R_\varepsilon = 1.00$, $\varepsilon_x = 0.001$ rad

1. The ratio between the two buckling loads: $R_{\mathrm{P}} = P_{\mathrm{cr},y}/P_{\mathrm{cr},x} = c_y/c_x$
2. The ratio between the imperfections in each direction: $R_\varepsilon = \varepsilon_y/\varepsilon_x$
3. The magnitude of initial imperfection in x-direction: ε_x

By substituting the selected values of R_{P}, R_ε and ε_x, the curves of Figs. 3 and 9 are obtained for seven different cases:

1. $R_{\mathrm{P}} = 1.00$, $R_\varepsilon = 1.00$, $\varepsilon_x = 0.001$ rad
2. $R_{\mathrm{P}} = 1.00$, $R_\varepsilon = 1.00$, $\varepsilon_x = 0.01$ rad
3. $R_{\mathrm{P}} = 1.00$, $R_\varepsilon = 0.25$, $\varepsilon_x = 0.01$ rad
4. $R_{\mathrm{P}} = 1.00$, $R_\varepsilon = 50$, $\varepsilon_x = 0.01$ rad
5. $R_{\mathrm{P}} = 0.25$, $R_\varepsilon = 0.25$, $\varepsilon_x = 0.01$ rad
6. $R_{\mathrm{P}} = 0.25$, $R_\varepsilon = 50$, $\varepsilon_x = 0.01$ rad
7. $R_{\mathrm{P}} = 0.25$, $R_\varepsilon = 1.00$, $\varepsilon_x = 0.01$ rad

The results are presented by means of equilibrium diagrams, shown in 3D (θ_x, θ_y, λ) form as well as in the form of 2D projections on the (θ_x, θ_y), (θ_x, λ), (θ_y, λ) planes, for easier comprehension of the system's response.

The post-buckling behavior of the system proves to be unstable in all cases, despite the stability of the two independent buckling modes. In the first case (Fig. 3), the system's response is entirely symmetric in both directions, as expected. Buckling mode interaction is activated at small values of deformation, rendering the response clearly unstable. Nevertheless, the limit point is observed at a value of λ, denoted a λ_{lp}, practically equal to 1. Thus, no significant strength reduction is observed and this because of the small magnitude of initial imperfections. This is verified by comparing the results with the case illustrated in Fig. 4, corresponding also to a symmetric system, but having 10 times larger initial imperfections. The structure's bearing capacity when $\varepsilon_x = 0.001$ rad is equal to $\lambda_{\mathrm{lp}} = 0.9868$ (Fig. 3), while in the case of $\varepsilon_x = 0.01$ rad (Fig. 4), the strength of the rod is equal

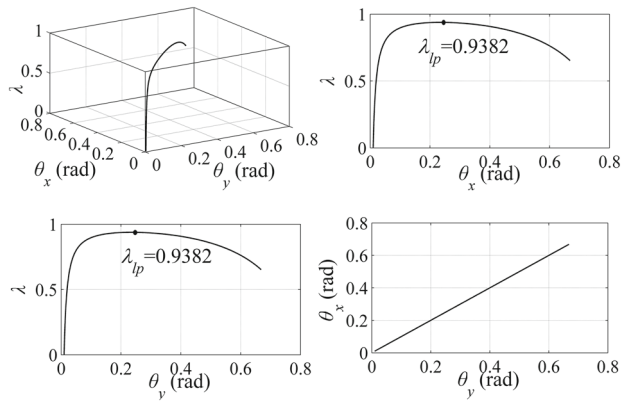

Fig. 4 Equilibrium paths of first 2-DOF model for $R_P = 1.00$, $R_\varepsilon = 1.00$, $\varepsilon_x = 0.01$ rad

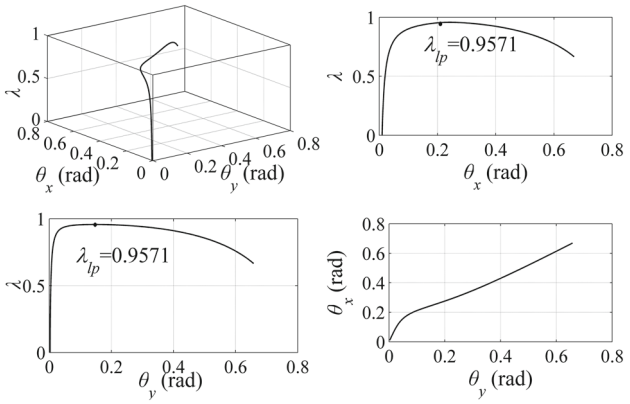

Fig. 5 Equilibrium paths of first 2-DOF model for $R_P = 1.00$, $R_\varepsilon = 0.25$, $\varepsilon_x = 0.01$ rad

to $\lambda_{lp} = 0.9382$. Thus, the reduction of the system's bearing capacity due to the increase of the initial imperfections is up to 5 %.

In Fig. 5, the two buckling loads are equal but the initial imperfection in x-direction is 4 times larger than the one in y-direction. The deformation is initially mainly in x-direction (θ_x rotation) due to the large initial disturbance, but afterward, the structure deforms almost the same in both directions. Similarly, in Fig. 6, the deformation in y-direction (θ_y rotation) dominates, while a significant reduction in the model's bearing capacity due to the large initial imperfection is observed.

In the fifth case (Fig. 7), the deformation in x-direction (θ_x rotation) dominates initially because of the larger associated imperfection, however eventually y-direction (θ_y rotation) attracts the response, which is the critical one, as it corresponds to a lower buckling load. It is noted, however, that this interaction is activated at very large values of deformation, as expressed by θ_y. The system's post-buckling response remains stable up to that level, denoting that in actual structural systems, where material nonlinearity will likely have developed at such high deformations, mode interaction would not be of practical significance.

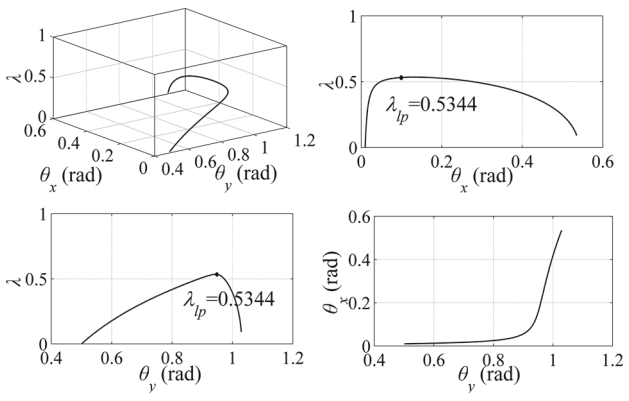

Fig. 6 Equilibrium paths of first 2-DOF model for $R_P = 1.00$, $R_\varepsilon = 50$, $\varepsilon_x = 0.01$ rad

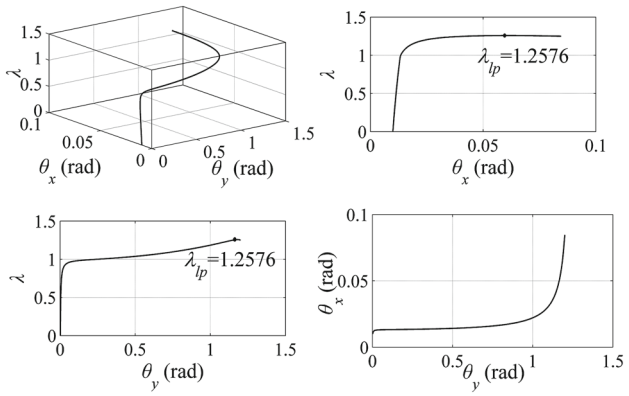

Fig. 7 Equilibrium paths of first 2-DOF model for $R_P = 0.25$, $R_\varepsilon = 0.25$, $\varepsilon_x = 0.01$ rad

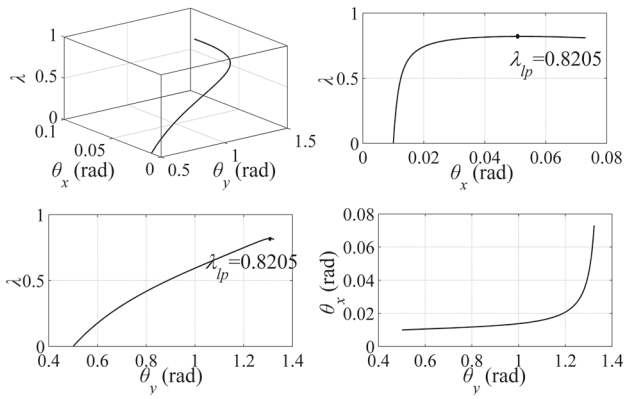

Fig. 8 Equilibrium paths of first 2-DOF model for $R_P = 0.25$, $R_\varepsilon = 50$, $\varepsilon_x = 0.01$ rad

In Fig. 8, the deformation in y-direction (θ_y rotation), which is the critical one, as it corresponds to a lower buckling load, dominates from the beginning due to the increased initial imperfection ε_y. As in the previous example (Fig. 7), the

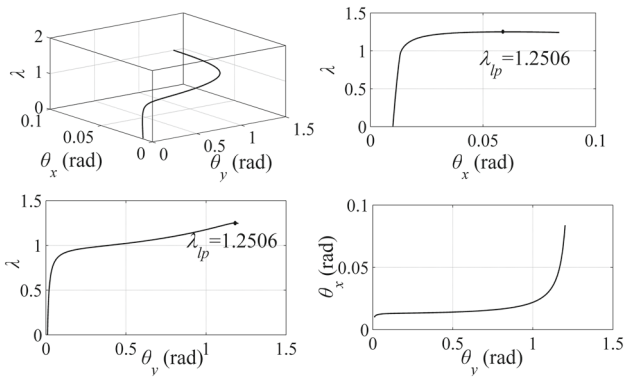

Fig. 9 Equilibrium paths of first 2-DOF model for $R_P = 0.25$, $R_\varepsilon = 1.00$, $\varepsilon_x = 0.01$ rad

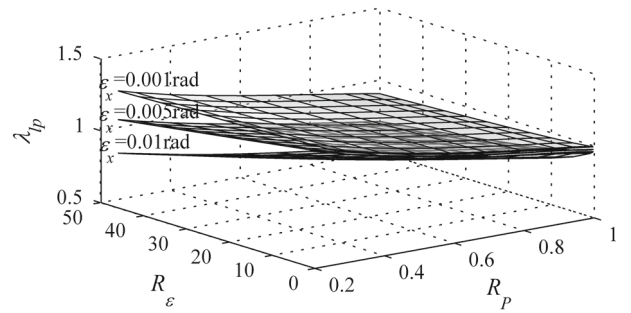

Fig. 10 Three-dimensional illustration of λ_{lp} with respect to R_ε and R_P for the first 2-DOF model

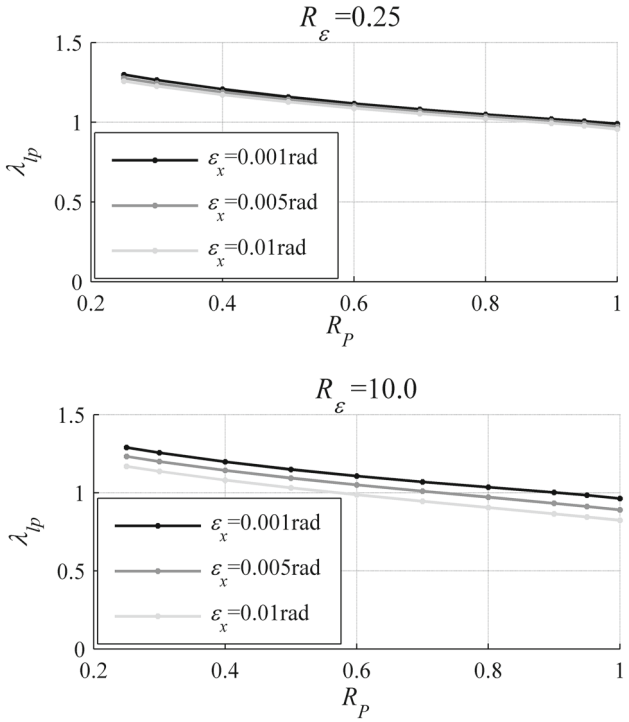

Fig. 11 Variation of λ_{lp} for constant R_ε (first 2-DOF model)

buckling mode interaction is activated at very large values of deformation θ_y.

In Fig. 9, the deformation in y-direction (θ_y rotation), which corresponds to the lower buckling load, dominates. Similarly to the previous examples (Figs. 7, 8), the model's coupled behavior is observed at very large values of deformation θ_y.

Following the qualitative understanding of the system's response for different values of the control parameters, a series of parametric studies are carried out in order to investigate the influence of coupling phenomena and initial imperfections on the model's behavior. The range of values of the control parameters, for which the parametric study is performed, is the following:

R_P: 0.25, 0.30, 0.40, 0.50, 0.60, 0.70, 0.80, 0.90, 0.95, 1.00
R_ε: 0.25, 0.50, 1.00, 5, 10, 15, 20, 25, 30, 35, 40, 45, 50
ε_x: 0.001 rad, 0.005 rad, 0.01 rad

A qualitatively similar behavior as in Figs. 3, 4, 5, 6, 7, 8 and 9 has been obtained for all combinations of values of the control parameters. In Fig. 10, the variation of the limit point load λ_{lp} with respect to the ratio of initial imperfections R_ε and the ratio of the two buckling loads R_P is presented in a three-dimensional graph. Each surface corresponds to a constant value of ε_x. The limit point load λ_{lp} represents the maximum load normalized with respect to the critical buckling load $P_{cr,y}$.

In Figs. 11 and 12, vertical sections of the above graph are illustrated in order to provide a deeper insight into the problem. In Fig. 11, the ratio between the initial imperfections R_ε is constant and the reduction of the structure's strength as R_P increases is demonstrated. In Fig. 12, the ratio between the buckling loads R_P remains fixed and the limit point load λ_{lp} with respect to R_ε is illustrated.

As the ratio between the buckling loads approaches unity, a stronger reduction of the system's bearing capacity due to the buckling mode interaction is observed. The limit point load λ_{lp} when $R_P = 0.25$, $R_\varepsilon = 50$, $\varepsilon_x = 0.01$ rad is equal to 0.82, while when $R_P = 1.00$, $R_\varepsilon = 50$, $\varepsilon_x = 0.01$ rad, λ_{lp} is equal to 0.53. It is also demonstrated, that as the initial imperfections increase, the phenomenon of coupled buckling becomes more intense. The increased imperfection sensitivity due to the buckling mode interaction is obvious. Finally, the reduction of the system's bearing capacity due to the increase of the initial imperfection ε_y, corresponding to the direction with the lower buckling load, is up to 45 % for the chosen values of the control parameters.

Then, a series of additional parametric studies are carried out in the region of $R_P = 1.00$, in order to demonstrate with more detail, the decrease of the column's bearing capacity when the two buckling loads interact. The range of values of

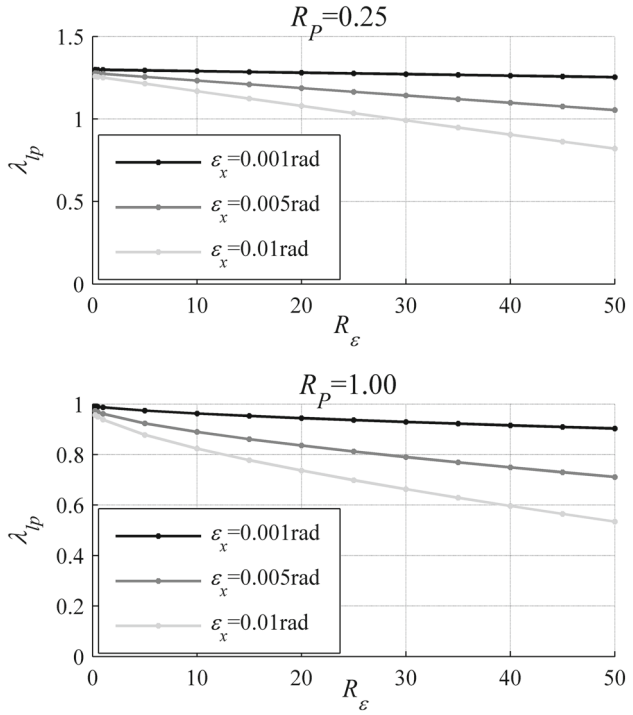

Fig. 12 Variation of λ_{lp} for constant R_P (first 2-DOF model)

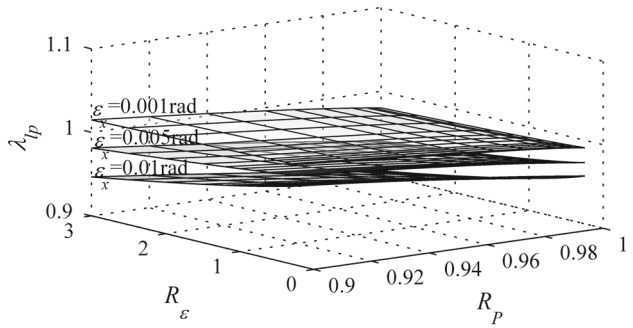

Fig. 13 Three-dimensional illustration of λ_{lp} with respect to R_ε and R_P in the region of $R_P = 1.00$ for the first 2-DOF model

the control parameters, for which the new parametric study is performed, is the following:

R_P: 0.90, 0.92, 0.94, 0.96, 0.97, 0.98, 0.99, 0.995, 0.997, 1.00
R_ε: 0.25, 0.30, 0.40, 0.50, 0.60, 0.80, 1.00, 1.20, 1.50, 2.00, 2.50, 3.00
ε_x: 0.001 rad, 0.005 rad, 0.01 rad

In Fig. 13, the variation of the limit point load λ_{lp} with respect to the ratio of initial imperfections R_ε and the ratio of the two buckling loads R_P is presented in a three-dimensional graph. Each surface corresponds to a constant value of ε_x.

In Figs. 14 and 15, vertical sections of the above graph are also illustrated. In Fig. 14, the ratio between the initial im-

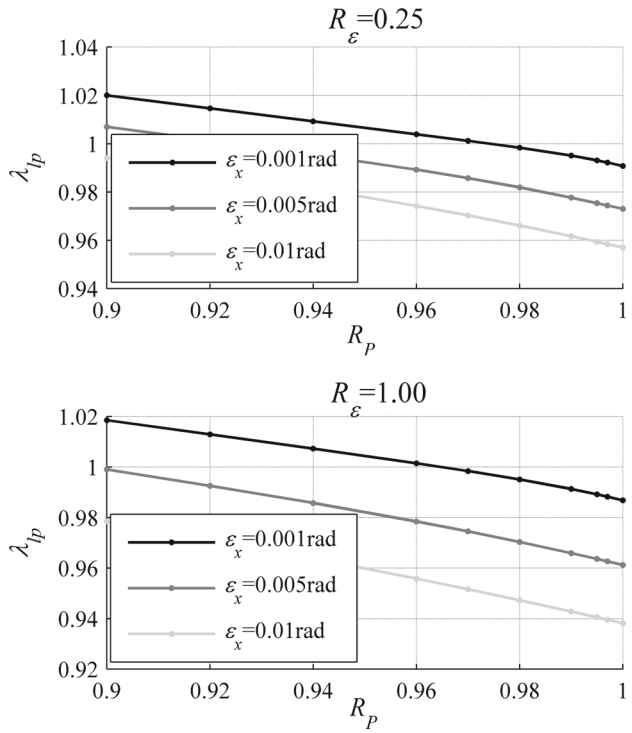

Fig. 14 Variation of λ_{lp} for constant R_ε in the region of $R_P = 1.00$ (first 2-DOF model)

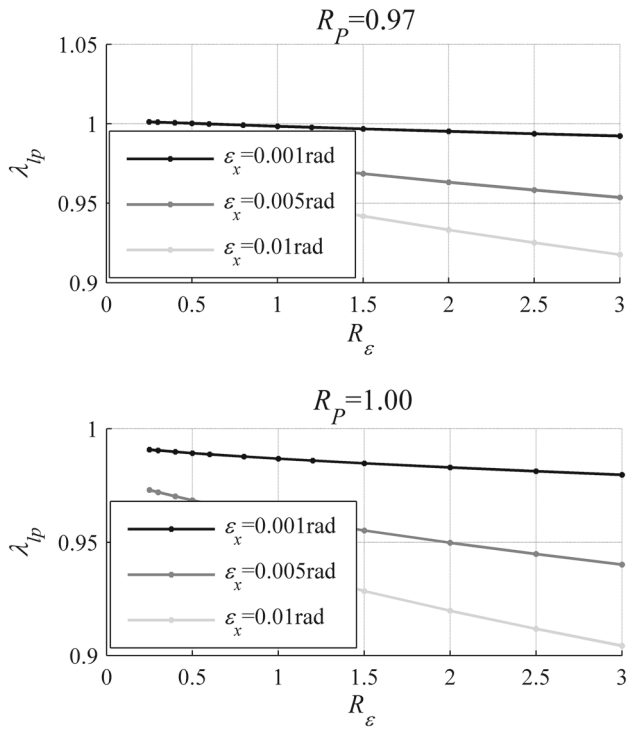

Fig. 15 Variation of λ_{lp} for constant R_P in the region of $R_P = 1.00$ (first 2-DOF model)

perfections R_ε is constant, while in Fig. 15, the ratio between the buckling loads R_P remains fixed.

2.3 Approximate Analytical Evaluation of the System's Bearing Capacity

By appropriate fitting of the above numerical results, an analytical expression has been derived for determining the system's strength with respect to the initial imperfection ε_x, the ratio between the initial imperfections R_ε and the ratio between the buckling loads R_P:

$$\lambda_{lp} = [-0.0069\ln(\varepsilon_x) + 1.353]\exp[-(3.2663\varepsilon_x + 0.3555)R_P]\exp(-\varepsilon_x R_\varepsilon) \quad (5)$$

The results obtained from Eq. (5) are very close to those derived from the numerical solution of the equilibrium equations. The maximum divergence between the two solutions is in the order of 7 %.

3 2-DOF Model with Stable Post-buckling Behavior

In the second model, the reactions of the rotational springs are chosen to be proportional to the angles BOC $= \theta'_x$ and BOD $= \theta'_y$ of the rod's projections on each plane with the vertical axis z (Fig. 16). In the case of initial imperfections, denoted by corresponding inclination ε'_x and ε'_y of the rod with respect to the vertical position, the springs are considered to be undeformed, thus their reactions are zero in the initial inclined position of the rod. The deformation is expressed with respect to the two rotational degrees of freedom θ'_x and θ'_y, and the equilibrium equations are derived by means of the energy method, accounting also for geometrical nonlinearities. In the following sections, the formulation of the model's equilibrium equations and their numerical treatment are presented.

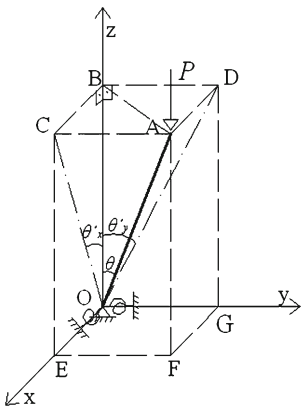

Fig. 16 Geometry of the second 2-DOF model

3.1 Formulation of Equilibrium Equations

The geometry of the model is demonstrated in Fig. 16. The springs exhibit linearly elastic response, with coefficients c'_x and c'_y in each direction, respectively. The critical loads of the two independent buckling modes of the system, which exhibit stable post-buckling response [14], are $P'_{cr,x} = c'_x/L$ and $P'_{cr,y} = c'_y/L$. In an arbitrary position, the rod forms with the vertical axis z angle equal to θ, the same as in the first example, while the corresponding initial angle is equal to ε.

By geometrical formulations, and without making any simplifying assumption, the exact relationship describing the geometry of the system is derived:

$$\cos\theta = \frac{1}{\sqrt{\tan^2\theta'_y + \tan^2\theta'_x + 1}} \quad (6)$$

The total potential energy Π of the system can then be written as:

$$\Pi = \frac{1}{2}c'_x\left(\theta'_x - \varepsilon'_x\right)^2 + \frac{1}{2}c'_y\left(\theta'_y - \varepsilon'_y\right)^2 - PL\left(\cos\varepsilon - \cos\theta\right) \quad (7)$$

By setting equal to zero, the derivatives of the total potential energy with respect to the two degrees of freedom θ'_x and θ'_y, and by normalizing the external force P with respect to the critical buckling load $P'_{cr,y} = c'_y/L$, the following equilibrium equations are obtained:

$$\frac{\partial\Pi}{\partial\theta'_x} = \frac{c'_x}{c'_y}(\theta'_x - \varepsilon'_x) - \lambda\frac{\tan\theta'_x\left(\cos\theta'_x\right)^{-2}}{\left(\tan^2\theta'_y + \tan^2\theta'_x + 1\right)^{3/2}} = 0 \quad (8)$$

$$\frac{\partial\Pi}{\partial\theta'_y} = (\theta'_y - \varepsilon'_y) - \lambda\frac{\tan\theta'_y\left(\cos\theta'_y\right)^{-2}}{\left(\tan^2\theta'_y + \tan^2\theta'_x + 1\right)^{3/2}} = 0 \quad (9)$$

where $\lambda = P/P'_{cr,y}$ is the normalized load. Each triad θ'_x, θ'_y, λ that satisfies the above equations, constitutes an equilibrium position of the system.

3.2 Numerical Treatment of Equilibrium Equations

The numerical solution of Eqs. (8), (9) was performed following the same process and selecting the same control parameters described in Sect. 2.2. By substituting the selected values of R_P, R_ε and ε'_x, the curves of Figs. 17 and 18 are obtained for two different cases:

1. $R_P = 1.00$, $R_\varepsilon = 1.00$, $\varepsilon'_x = 0.001$ rad
2. $R_P = 0.25$, $R_\varepsilon = 0.25$, $\varepsilon'_x = 0.001$ rad

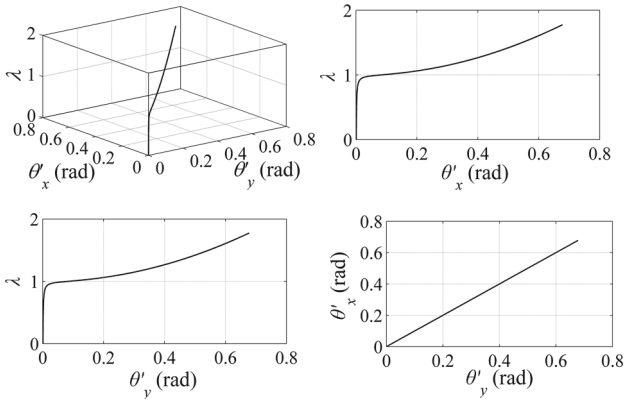

Fig. 17 Equilibrium paths of second 2-DOF model for $R_P = 1.00$, $R_\varepsilon = 1.00$, $\varepsilon'_x = 0.001$ rad

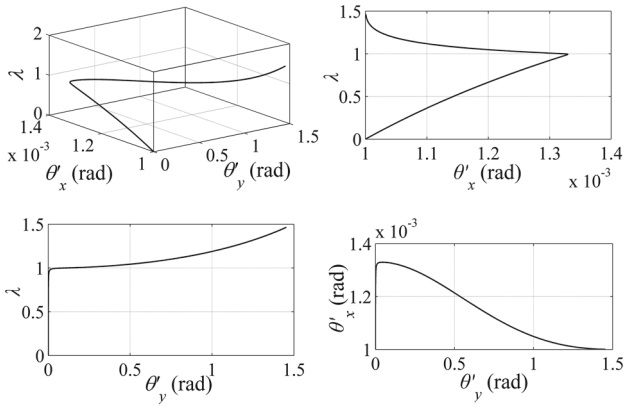

Fig. 18 Equilibrium paths of second 2-DOF model for $R_P = 0.25$, $R_\varepsilon = 0.25$, $\varepsilon'_x = 0.001$ rad

The post-buckling behavior of the 2-DOF system proves to be stable for all chosen values of the control parameters. In the first case (Fig. 17), the system's response is totally symmetric in both directions, as expected. In the second case (Fig. 18), the rod is initially deformed mainly in x-direction due to the increased initial imperfection ε'_x, but subsequently the deformation in y-direction dominates, which is the critical one, as it corresponds to a lower buckling load. In such systems, whose post-buckling equilibrium paths are stable, the effect of initial imperfections proves to be insignificant for the elastic post-buckling response beyond a certain load level.

4 First Example of Built-Up Column: In-Plane Behavior

Built-up columns are well known for exhibiting buckling mode interaction and imperfection sensitivity. The effect of the interaction between global and local buckling in built-up members has been investigated by many researchers, among them by Bažant and Cedolin [1], Svensson and Kragerup [19], Miller and Hedgepeth [20] and recently by Kalochairetis and Gantes [21]. In this example, a simply supported laced built-up column under compressive load is investigated, in order to demonstrate the buckling mode interaction between the local buckling of the flanges and the in-plane global buckling, considering linearly elastic material behavior. The geometry and the section properties of the system are shown in Fig. 19.

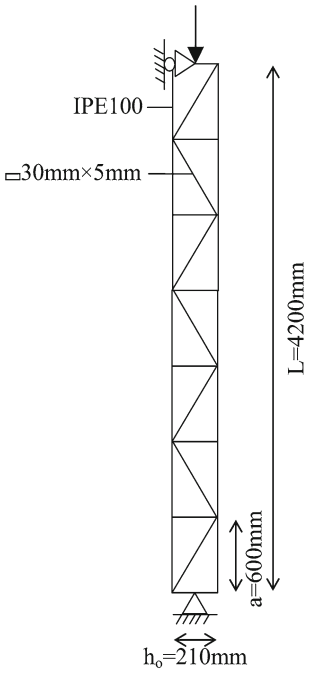

Fig. 19 First examined built-up column

4.1 Critical Buckling Loads

The buckling loads of the in-plane global and flanges local buckling are first calculated according to the EC3 provisions [22] concerning built-up columns. Global buckling of the member occurs at load level:

$$P_{\mathrm{cr,g,EC3}} = \frac{1}{\frac{1}{P_\mathrm{E}} + \frac{1}{S_\mathrm{V}}} = 1{,}894\,\mathrm{kN} \tag{10}$$

where P_E is the Euler critical buckling load and S_V the shear rigidity of the built-up column. The Euler critical load is given by:

$$P_\mathrm{E} = \frac{\pi^2 E I_\mathrm{eff}}{(kL)^2} = 2{,}674\,\mathrm{kN} \tag{11}$$

where EI_eff is the effective bending rigidity of the column and k the effective length factor. The effective bending rigidity is primarily due to the Steiner term of the moment of inertia of the cross-section and is given by:

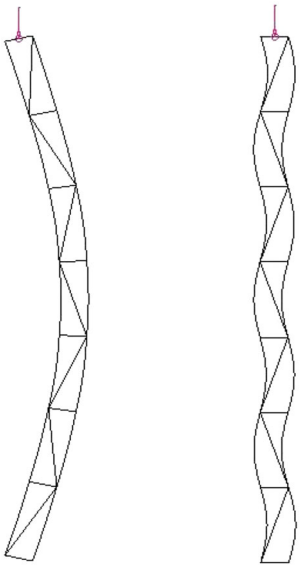

Fig. 20 Global and local in-plane buckling modes of built-up column from FEM linearized buckling analysis (first example)

$$EI_{\text{eff}} = 0.5h_o^2 EA_{\text{ch}} = 4{,}779\,\text{kNm}^2 \tag{12}$$

The shear rigidity of the considered laced built-up column is equal to:

$$S_{\text{V}} = \frac{nEA_{\text{d}}ah_{\text{o}}^2}{d^3} = 6{,}490\,\text{kN} \tag{13}$$

where n is the number of the planes of lacing, A_{d} is the cross-sectional area of the lacing bars and d is the length of diagonal elements.

The column's flanges buckle as a simply supported rod and therefore, local buckling occurs at the load level:

$$P_{\text{cr,l,EC3}} = 2\frac{\pi^2 EI_{\text{ch},z}}{a^2} = 1{,}833\,\text{kN} \tag{14}$$

The ratio between the two buckling loads calculated according to EC3 can then be obtained as:

$$n = \frac{P_{\text{cr,g,EC3}}}{P_{\text{cr,l,EC3}}} = 1.03 \tag{15}$$

Similar results are obtained making use of software ADINA. After performing a linearized buckling analysis, the derived buckling loads are $P_{\text{cr,g,FEM}} = 1{,}812\,\text{kN}$ and $P_{\text{cr,l,FEM}} = 1{,}861\,\text{kN}$. Thus, the ratio between the numerically calculated buckling loads is obtained as:

$$n = \frac{P_{\text{cr,g,FEM}}}{P_{\text{cr,l,FEM}}} = 0.97 \tag{16}$$

The corresponding buckling modes are shown in Fig. 20.

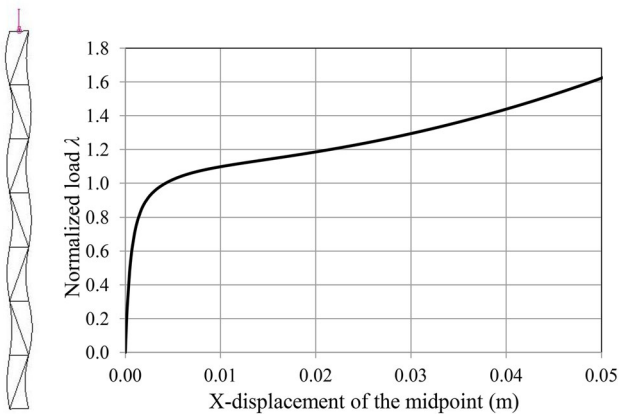

Fig. 21 Equilibrium path and deformation of local buckling of built-up column (first example)

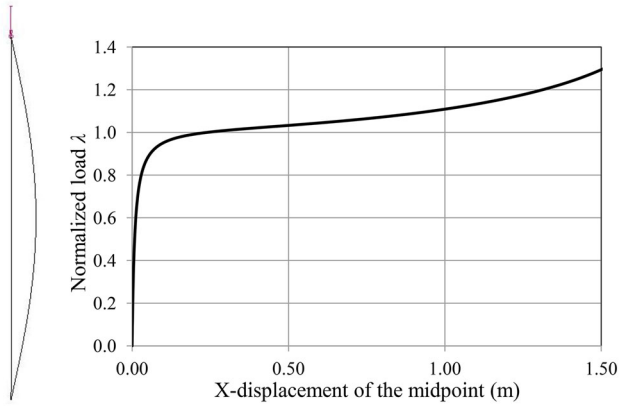

Fig. 22 Equilibrium path and deformation of in-plane global buckling of built-up column (first example)

4.2 Geometrically Nonlinear Finite Element Analyses

In the present section, geometrically nonlinear elastic analyses in the presence of initial imperfections (GNIA) are performed with the finite element software ADINA, in order to investigate the stability of the column's post-buckling equilibrium path. The two independent buckling modes exhibit stable post-buckling behavior, as shown in Figs. 21 and 22. The vertical axis represents the load normalized with respect to the local (Fig. 21) or global (Fig. 22) buckling load, respectively. In order to avoid global buckling, the horizontal displacement of the lacing joints of flanges is restrained. Thus, the column's flanges are allowed to buckle locally. On the other hand, local buckling was prevented by modeling the equivalent solid section of the built-up column, accounting also for the effect of shear deformations, so that all local buckling phenomena are eliminated.

Subsequently, the coupled behavior of the column is investigated. The imposed global and local imperfections are chosen to be equal to the buckling length divided by 500. Thus, global imperfection is equal to $\varepsilon_{\text{g}} = \text{L}/500 = 8.4\,\text{mm}$

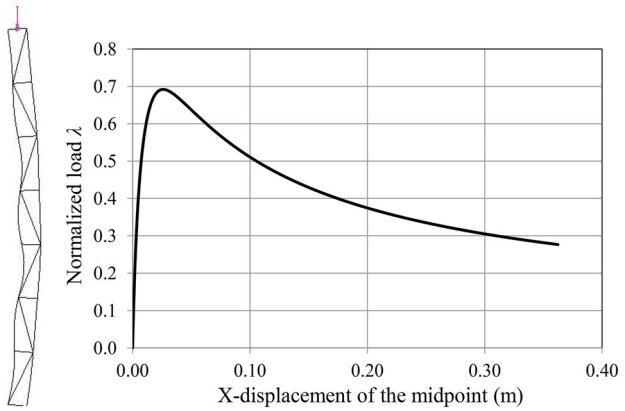

Fig. 23 Equilibrium path and deformation of built-up column exhibiting interaction between local and in-plane global buckling (first example)

(according to the first buckling mode) and local imperfection is equal to $\varepsilon_l = a/500 = 1.2$ mm (according to the second buckling mode), respectively. The vertical axis represents the load normalized with respect to the global buckling load. The post-buckling equilibrium path proves to be unstable despite the stability of both independent buckling modes, as shown in Fig. 23. From the deformed shape at the limit point, it is evident that failure is characterized by coupling of local and global buckling. The limit point load is approximately equal to 70 % of the first critical buckling load for the chosen initial imperfections. The post-buckling response of the considered built-up column is similar to the corresponding one of the first among the two studied 2-DOF models.

Then, a series of parametric analyses are carried out in order to investigate the influence of coupling phenomena and initial imperfections on the column's behavior. The control parameters are the ratio between the buckling loads $n = P_{\mathrm{cr,g,FEM}}/P_{\mathrm{cr,l,FEM}}$, as well as the global and local initial imperfections. The change of ratio n is achieved by variation of the section properties of the flanges. The range of values of the control parameters, for which the analyses are performed, is the following:

n: 0.50, 0.67, 0.91, 0.97, 0.99, 1.00, 1.02, 1.04, 1.15, 1.52, 1.92
ε_l: 0, 0.0006 m, 0.0012 m, 0.0024 m
ε_g: 0.0021 m, 0.0042 m, 0.0084 m, 0.0168 m

The built-up column exhibits unstable post-buckling behavior for all values of the control parameters. In Fig. 24, the variation of the limit point load normalized with respect to the minimum buckling load is presented in a three-dimensional graph for a wide range of values of the ratio n between the two buckling loads and the local initial imperfection ε_l. Each

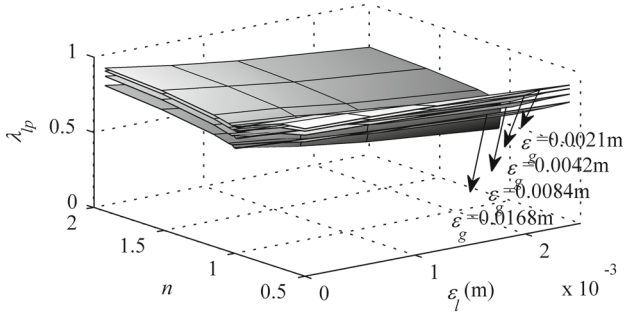

Fig. 24 Three-dimensional illustration of limit point load λ_{lp} with respect to the buckling loads ratio n and the local imperfection ε_l for the first built-up column (in-plane behavior)

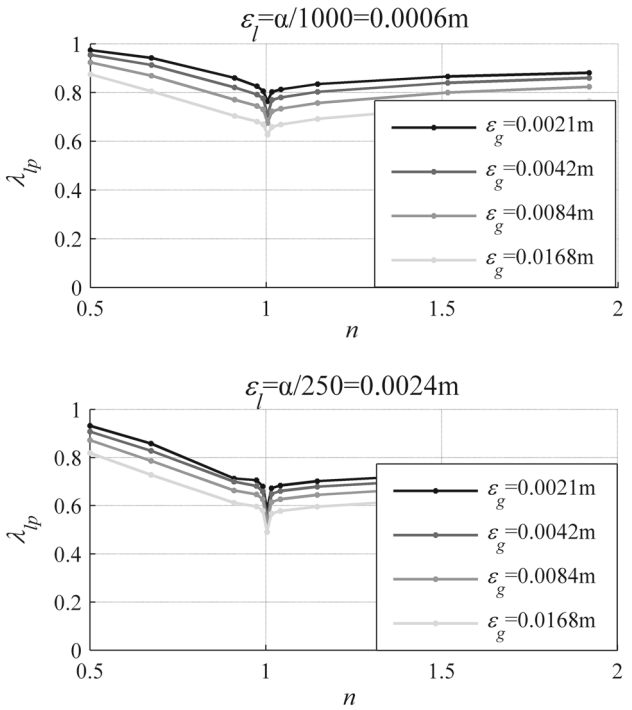

Fig. 25 Variation of λ_{lp} for constant ε_l for the first built-up column (in-plane behavior)

surface corresponds to a constant value of the global initial imperfection ε_g.

In addition, vertical sections of the above graph are plotted in order to provide a deeper insight into the problem. In Fig. 25, the initial imperfection ε_l is constant and the limit point load λ_{lp} with respect to buckling loads' ratio n is demonstrated in a two-dimensional graph. In Fig. 26, the ratio n between the buckling loads remains constant and the limit point load λ_{lp} with respect to the local initial imperfection ε_l is presented.

Then, the imperfection sensitivity diagrams are demonstrated in Fig. 27. The vertical axis represents the limit point load $P_{\max}$ normalized with respect to the local buckling load

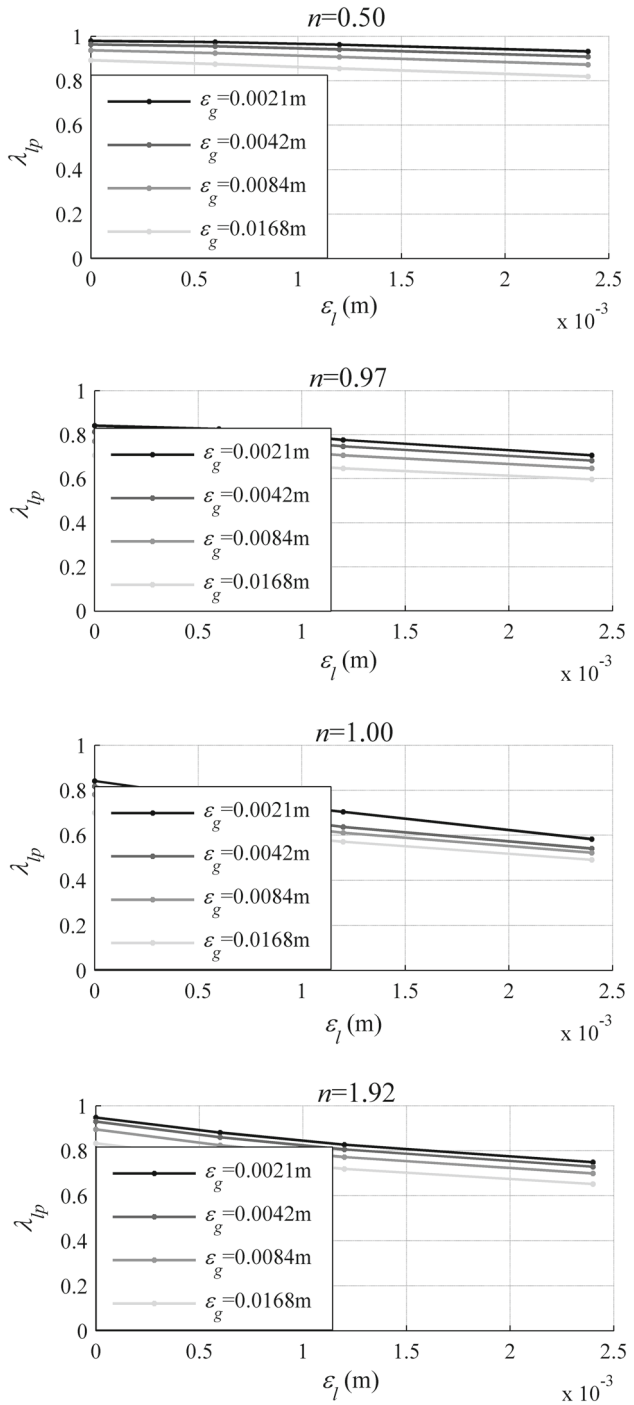

Fig. 26 Variation of λ_{lp} for constant n for the first built-up column (in-plane behavior)

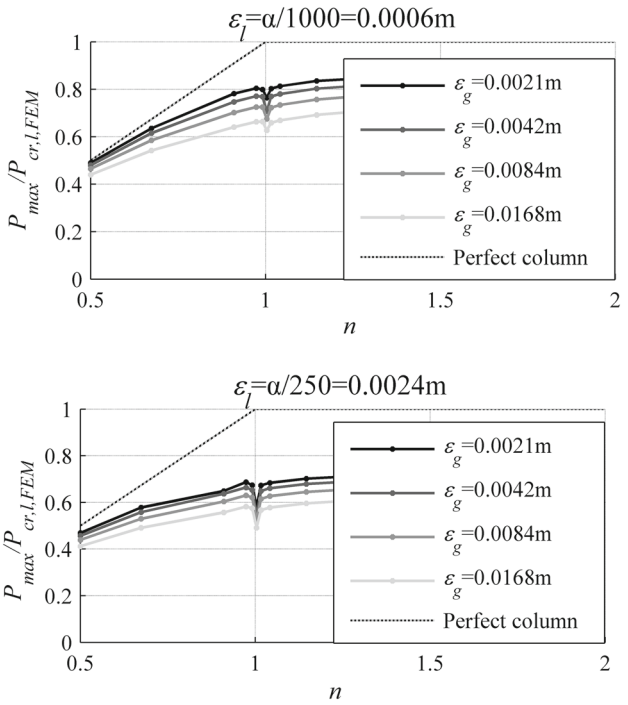

Fig. 27 Imperfection sensitivity diagrams for the first built-up column (in-plane behavior)

$P_{cr,l,FEM}$, while the horizontal axis represents the buckling modes ratio n.

Based on this parametric study, it can be concluded that as the ratio between the buckling loads n approaches unity, the system's bearing capacity decreases due to buckling mode interaction. The limit point load λ_{lp} when $n = 0.50$, $\varepsilon_l = 0.0024$m, $\varepsilon_g = 0.0168$ m is equal to 0.82, while when $n = 1.00$, $\varepsilon_l = 0.0024$ m, $\varepsilon_g = 0.0168$ m, λ_{lp} is equal to 0.49. It is also demonstrated that local buckling is more critical than in-plane global buckling for such columns. The coupling phenomena are more intense when the local buckling load is smaller than the global one, accompanied by a larger reduction in the column's bearing capacity. The effect of global initial imperfections remains similar for all values of control parameters, even if the two buckling loads interact. Lastly, the column proves to be very sensitive to the increase of the local initial imperfection, leading to a decrease of the structure's strength up to 34 %. This sensitivity becomes more intense as the ratio n approaches unity.

5 Second Example of Built-Up Column: In- and Out-of-Plane Behavior

In the second example, a similar built-up column with different section properties is studied but out-of-plane deformations are now allowed. The geometry and section of the flanges are appropriately chosen in order to avoid in-plane local buckling. Thus, interaction between in-plane and out-of-plane global buckling is investigated. The column is simulated by its equivalent solid section taking into consideration the effect of the in-plane shear deformations, in order to avoid any local buckling phenomena that could modify the system's response.

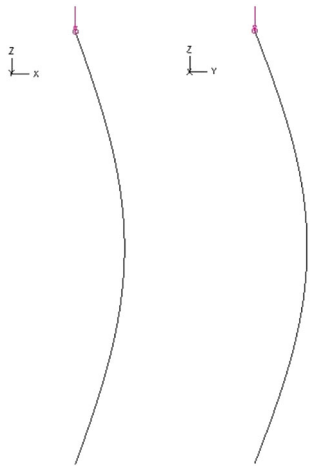

Fig. 28 In-plane and out-of-plane global buckling modes of built-up column from FEM linearized buckling analysis (second example)

5.1 Critical Buckling Loads

Performing a linearized buckling analysis using the software ADINA, the derived buckling loads are $P_{\mathrm{cr},x} = 6{,}985\,\mathrm{kN}$, representing in-plane global buckling, and $P_{\mathrm{cr},y} = 7{,}011\,\mathrm{kN}$ associated with out-of-plane global buckling. Therefore, the ratio between the buckling loads is obtained equal to:

$$m = \frac{P_{\mathrm{cr},x}}{P_{\mathrm{cr},y}} = 1.00 \tag{17}$$

The corresponding buckling modes are shown in Fig. 28.

5.2 Geometrically Nonlinear Finite Element Analyses

Subsequently, geometrically nonlinear analyses are performed in order to investigate the stability of the column's post-buckling equilibrium path. The two independent global buckling modes exhibit stable post-buckling behavior, as has been shown for the in-plane case in Sect. 4.2 (Fig. 22). A series of parametric analyses are carried out in order to examine the effect of buckling mode interaction and initial imperfections on the system's response. The control parameters are the ratio between the buckling loads $m = P_{\mathrm{cr},x}/P_{\mathrm{cr},y}$, and the in-plane and out-of-plane global initial imperfection, ε_x and ε_y, respectively. The change of the ratio m is achieved by variation of the flanges section properties. The values of the control parameters, for which the analyses are performed, are the following:

1. m: 0.55, 1.00, 1.99
2. ε_x: 0, 0.0042 m, 0.0084 m
3. ε_y: 0.0021 m, 0.0042 m, 0.0084 m

In Figs. 29, 30 and 31, the system's post-buckling equilibrium paths for different values of the control parameters

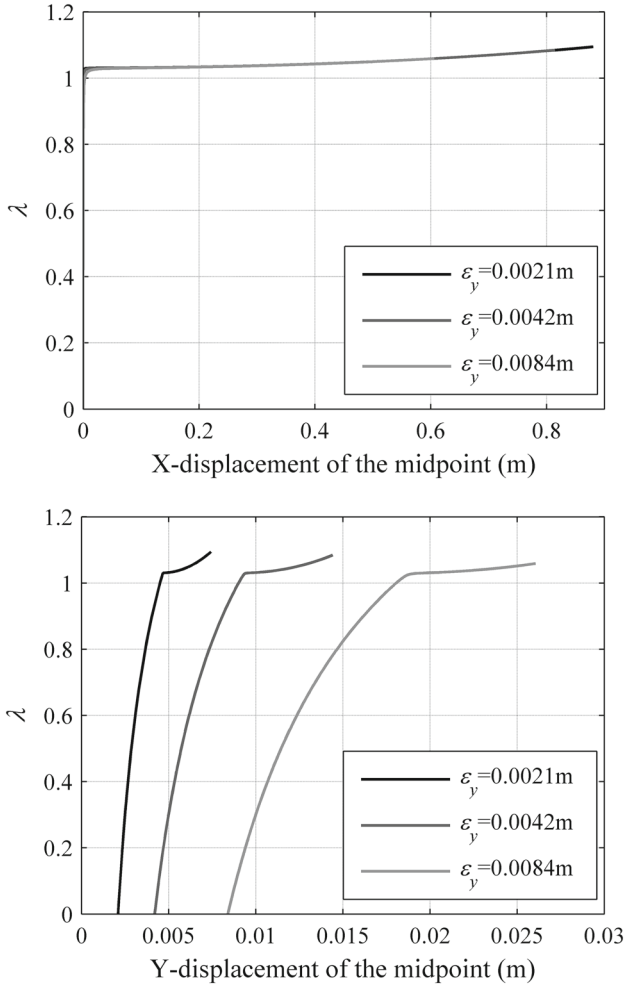

Fig. 29 Equilibrium paths for constant values $m = 0.55$ and $\varepsilon_x = 0$ (second example)

are demonstrated. The vertical axis represents the load normalized with respect to the first buckling load. Each curve corresponds to a different value of the out-of-plane global initial imperfection ε_y.

In contrast to the previous example, the post-buckling behavior of the second built-up column proves to be stable for all values of the control parameters, similarly to the second 2-DOF model discussed in Sect. 3. Thus, the influence of the magnitude of initial imperfections on the system's elastic post-buckling response is insignificant above a certain load level. In addition, the coupling phenomena prove to be incapable of modifying the equilibrium path's stability. In any case, the deformation in the critical direction, which corresponds to the minimum buckling load, dominates.

6 Summary and Conclusions

The well-known fact that two independent stable buckling modes can interact in the presence of imperfections has been

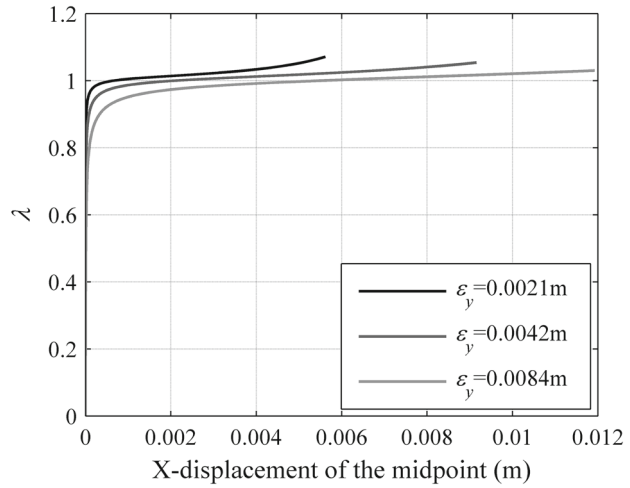

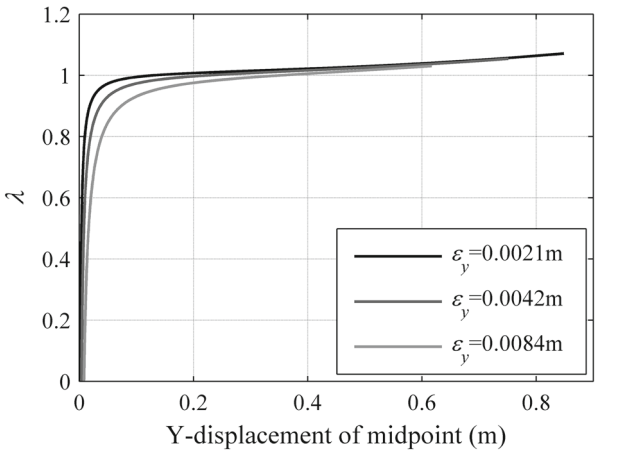

Fig. 30 Equilibrium paths for constant values $m = 1.00$ and $\varepsilon_x = 0$ (second example)

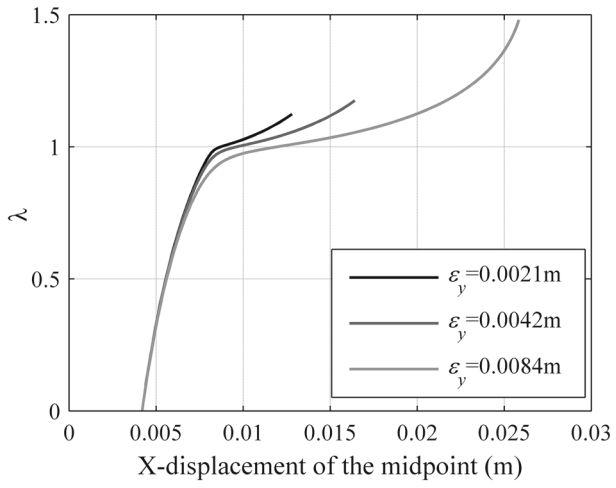

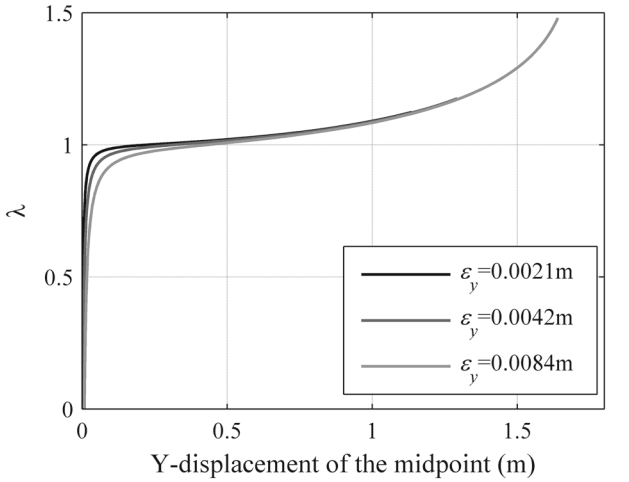

Fig. 31 Equilibrium paths for constant values $m = 1.99$ and $\varepsilon_x = 0.0042$ m (second example)

first demonstrated for simple 2-DOF structural systems derived from Augusti's model. By employing large displacement analysis and avoiding mathematical simplifications that are commonly adopted in pertinent studies, it has been shown that this interaction may result either in stable or unstable post-buckling response.

This is then verified by two examples of built-up columns, a structural typology which is well known to exhibit buckling mode interaction. Depending on the kind of the coupled buckling modes, the column's elastic post-buckling equilibrium path can be either stable or unstable. In the case of instability, encountered for coupling between global and local in-plane modes, the buckling mode interaction leads to a significant reduction of the system's bearing capacity, which is accompanied by increased imperfection sensitivity. In the case of stability, exhibited for coupling between in- and out-of-plane global buckling modes, the effect of coupling phenomena and imperfections proves to be insignificant and incapable of modifying the equilibrium path's stability. It should be noted that material nonlinearity, which is an additional very important factor for determining bearing capacity of built-up columns, has not been taken into account in this investigation.

References

1. Bažant, Z.P.; Cedolin, L.: Stability of Structures. Oxford University Press, Oxford (1991)
2. Chilver, A.H.: Coupled modes of elastic buckling. J. Mech. Phys. Solids **15**, 15–28 (1967)
3. Koiter, W.T.: On the stability of elastic equilibrium. Dissertation, Holland, Delft (1945)
4. Supple, W.J.: Coupled branching configurations in the elastic buckling of symmetric structural systems. Int. J. Mech. Sci. **9**, 97–112 (1967)
5. Johns, K.C.; Chilver, A.H.: Multiple path generation at coincident branching points. Int. J. Mech. Sci. **13**, 889–910 (1971)
6. Roorda, J.: Stability of structures with small imperfections. J. Eng. Mech. Div. (ASCE) **91**(1), 87–106 (1965)
7. Ho, D.: Higher order approximations in the calculation of elastic buckling loads of imperfect systems. Int. J. Non Linear Mech. **6**, 649–661 (1971)

8. Thompson, J.M.T.: A new approach to elastic branching analysis. J. Mech. Phys. Solids **18**, 29–42 (1970)
9. Supple, W.J.: Initial post-buckling behaviour of a class of elastic structural systems. Int. J. Non Linear Mech. **4**, 23–36 (1969)
10. Ho, D.: The influence of imperfections on systems with coincident buckling loads. Int. J. Non Linear Mech. **7**, 311–321 (1972)
11. Ho, D.: Buckling load of non-linear systems with multiple eigenvalues. Int. J. Solids Struct. **10**, 1315–1330 (1974)
12. Johns, K.C.: Imperfection sensitivity of coincident buckling systems. Int. J. Non Linear Mech. **9**, 1–21 (1974)
13. Gioncu, V.: General theory of coupled instabilities. Thin Wall. Struct. **19**, 81–127 (1994)
14. Augusti, G.: Stabilita di strutture elastiche elementari in presenza di grandi spostamenti. Atti dell' Accademia Scienze fisiche e matematiche. Napoli **4**(5) (1964)
15. ADINA system 8.5. Release Notes. ADINA R&D Inc. (2008)
16. Livanou, M.A.; Gantes, C.J.; Avraam, T.P.: Revisiting the problem of buckling mode interaction in 2-DOF models and built-up columns. In: Obre bski, J.B.; Tarczewski, R. (eds.) Proceeding of International Association for Shell and Spatial Structures (IASS) Symposium. "Beyond the Limits of Man", Wroclaw (2013)
17. MATLAB R2008b. The MathWorks Inc. (2008)
18. Crisfield, M.A.: A fast incremental/iterative solution procedure that handles "snap-through". Comput. Struct. **13**, 55–62 (1981)
19. Svensson, S.E.; Kragerup, J.: Collapse loads of laced columns. J. Struct. Div. (ASCE) **108**(ST6), 1367–1384 (1982)
20. Miller, R.K.; Hedgepeth, J.M.: The buckling of lattice columns with stochastic imperfections. Int. J. Solids Struct. **15**, 73–84 (1979)
21. Kalochairetis, K.E.; Gantes, C.J.: Numerical and analytical investigation of collapse loads of laced built-up columns. Comput. Struct. **89**, 1166–1176 (2011)
22. Eurocode 3: Design of steel structures. Part 1.1: General structural rules. CEN-European Committee for Standardisation. EN1993-1-1. Brussels (2002)